A Study on the Efficient Separation of Oily Water Using Mullite Whiskers Membrane through Combined Filtration and Electrofiltration

M. Naseri [a], S. F. Mousavi [b], M. R. Omidkhah [a, *]

[a, *] Process Engineering Department, Faculty of Chemical Engineering, Tarbiat Modares University, Tehran, Iran.

[b] School of Chemical, Petroleum and Gas Engineering, Iran University of Science and Technology, Tehran, Iran.

Abstract

Oily wastewaters pose significant environmental challenges, requiring effective treatment methods for sustainable development. This study investigates the potential of combining filtration, electrofiltration, and backwashing using a ceramic membrane for the treatment of oily water. A secondary mullite membrane is synthesized, demonstrating favorable characteristics such as high permeate flux (534 LMH), biaxial flexural strength (75.21 MPa), and cost-effectiveness. Experimental investigations were performed for operational parameters, resulting in the selection of a pressure of 2 bar and a cross-flow velocity of 0.727 m/s to achieve desirable permeate flux and oil removal rates. The critical electric field intensity (E_{crit}) is determined experimentally and theoretically, ranging from 50 to 55 V, guiding the selection of optimal voltages for electrofiltration. Electrokinetic phenomena, including electrophoresis, electroosmosis, and bubble formation, are harnessed to mitigate fouling. The influence of feed solution conductivity is examined, revealing that higher salt concentrations increase fouling and diminish electric field effectiveness. Energy consumption analysis indicates significant potential for energy savings, with a decrease from 3.88 kWh/m³ in the no-voltage condition to 2.71 kWh/m³ at 65 V for salt-free solutions. However, at higher salt concentrations, increased fouling and reduced electric field effectiveness result in higher energy consumption. The findings underscore the suitability of low-cost ceramic membranes for oily water treatment, emphasizing the importance of optimizing operating parameters for enhanced performance and energy efficiency.

Keywords

Mullite whiskers, Ceramic membrane, Oily water emulsion, Electrofiltration, Membrane fouling, Energy consumption

1. Introduction

Oily wastewaters pose significant environmental challenges, affecting both terrestrial and aquatic ecosystems. The discharge of these wastewater streams from various industries, such as oil refineries, petrochemical plants, and offshore drilling operations, not only degrades water quality but also threatens biodiversity and human health. As the demand for oil continues to grow, the proper treatment and management of oily wastewaters have become increasingly

important for sustainable development and the well-being of future generations (Al-Kaabi et al., 2021; Coca et al., 2011; Salahi et al., 2010).

Various treatment methods have been employed to address the challenges associated with oily water treatment, including physical, chemical, and biological processes (Ahmed et al., 2021; Zhao et al., 2021). However, these methods often have limitations, such as high operating costs, complex operations, and the generation of secondary pollutants (Eom et al., 2014). In recent years, membrane-based separation techniques have gained significant attention due to their high efficiency, simplicity, and potential for integration into existing treatment systems (Davoodbeygi et al., 2023; Goh et al., 2022).

Among membrane materials, ceramic membranes have shown great promise for oily water treatment due to their unique properties. Ceramic membranes are known for their exceptional thermal and chemical stability, mechanical strength, and resistance to fouling (Dong et al., 2022; Gu et al., 2022; Li et al., 2020). These characteristics make them well-suited for harsh operating conditions and the removal of oil droplets, suspended solids, and other contaminants from wastewater streams. However, the high cost of ceramic membrane production has hindered their widespread adoption in industrial applications (Hubadillah et al., 2017).

In addressing the cost issue, researchers have explored strategies such as utilizing low-cost raw materials, innovative fabrication techniques, and optimizing manufacturing processes to reduce production costs while preserving the performance and durability of ceramic membranes. These approaches enhance the economic feasibility of ceramic membranes for oily water treatment, increasing their practical implementation (Guo et al., 2016; Naseri and Omidkhah, 2023; Zhu et al., 2016; Zou et al., 2019). Notably, mullite whiskers membranes hold promise for reducing production costs while maintaining or even enhancing properties like biaxial flexural strength and porosity. With their cost-effective production and favorable characteristics, mullite whiskers membranes offer an opportunity to enhance the economic viability of ceramic membranes for industrial applications in oily water treatment (Abdullayev et al., 2022; Fu et al., 2019; Naseri and Omidkhah, 2023).

Another critical challenge associated with membrane technology, which directly impacts cost and consumed energy, is fouling. The occurrence and accumulation of fouling on membrane surfaces pose significant obstacles to efficient filtration and necessitate the implementation of effective fouling mitigation strategies. Fouling can significantly affect the performance and lifespan of membranes (Akhondi et al., 2014; Nthunya et al., 2022). In the context of oily water treatment, fouling is primarily attributed to the deposition of oil droplets, organic matter, and other contaminants on the membrane surface, leading to flux decline and reduced separation efficiency (Campo et al., 2017; Ullah et al., 2021). To combat fouling and enhance membrane performance, electrofiltration has emerged as a promising technique (Chiu and Garcia Garcia, 2011; Khosravanipour Mostafazadeh et al., 2016).

Electrofiltration harnesses the application of an electric field across the membrane to improve separation efficiency and mitigate fouling. This technique capitalizes on various electrokinetic phenomena, such as electrophoresis, electroosmosis, and bubble formation, to enhance particle removal and minimize membrane fouling (Khosravanipour Mostafazadeh et al., 2016; Shen and Badireddy, 2021). By positioning the membrane between two electrodes, electrofiltration facilitates the migration of charged particles towards the oppositely charged electrode,

preventing their accumulation on the membrane surface (Chiu and Garcia Garcia, 2011; Huotari et al., 1999b; Shen and Badireddy, 2021).

In the configuration where the membrane is placed between two electrodes, so far, organic membranes such as polyvinylidene difluoride (PVDF) (Du et al., 2013; Du et al., 2009; Hu et al., 2019; Huang et al., 2015; Oussedik et al., 2000; Sun et al., 2017; Yang et al., 2003; Zhang et al., 2017), polyethersulfone (PES) (Sarkar and De, 2011; Venkataganesh et al., 2012; Weng et al., 2006), polysulfone (PS) (Sarkar et al., 2008; Song et al., 2010), polyacrylonitrile (PAN) (Lee et al., 2008), polypropylene (PP) (Chen et al., 2007), and nylon (Sarkar, 2015) have been used. Furthermore, some studies have focused on the use of inorganic membranes, particularly ceramic membranes, with more details provided. Chiu et al. (Chiu and Garcia Garcia, 2011) utilized a commercial star-shaped ceramic membrane for the electrofiltration of activated sludge suspension in wastewater treatment. They obtained a critical electric field intensity (E_{crit}) ranging from 30 to 45 V/cm and achieved a maximum separation percentage of approximately 90%. Agana et al. (Agana et al., 2012) employed electro-ultrafiltration for treating wastewater containing 5% volume of CED dye used in automobile paint shop baths. They observed that different voltage differentials generally improved filtration under a working pressure of 100 kPa, with the highest impact seen at 60 V. Chiu et al. also used a star-shaped industrial membrane for whey suspension treatment in another study (Chiu, 2013). They reported E_{crit} ranging from 12.5 to 15 V/cm. The effect of direct current electric field on flux in crossflow filtration using a tubular membrane was investigated by Kyllönen et al. (Kyllönen, 2005). They concluded that even low-velocity flows can be utilized for electrofiltration.

The aim of this study is to design a practical membrane process in the field of combined filtration, electrofiltration, and backwashing for the treatment of crude oil/water emulsion, building upon our previous work optimizing the synthesis conditions of secondary mullite membrane, which has exhibited excellent characteristics in terms of permeance, biaxial flexural strength, and cost-effectiveness (Naseri and Omidkhah, 2023). The ultimate goal is to develop a process that achieves the best efficiency in terms of permeate flux, removal rate, and energy consumption, using an affordable and optimized ceramic membrane. To achieve this, the impact of operational parameters, including pressure, cross-flow velocity, backwashing, and electric field strength, on membrane performance has been investigated. Furthermore, the influence of feed solution conductivity on the electrofiltration process has been examined.

2. Experimental procedures

2.1. Materials and synthesis methods

In our previous work (Naseri and Omidkhah, 2023), we focused on optimizing the fabrication conditions of a secondary mullite ceramic membrane. Briefly, here we refer to the optimized membrane fabrication conditions mentioned in that work. As shown in Fig. 1, kaolin and bauxite were used as the main materials, along with $AlF_3.3H_2O$ and MoO_3 as additives in stoichiometric proportions of mullite ($3Al_2O_3.2SiO_2$). To homogenize the powder, a planetary mill was used at a speed of 250 rpm for 4 hours. Afterwards, the obtained slurry was placed in an oven at 80°C for 3 hours and left to be dry at room temperature for one day. Then, 1% by weight of a 5% PVA solution was added to the slurry and thoroughly mixed. Subsequently, the final powder was passed through stainless steel sieves to obtain a fine powder with suitable and uniform particle size for pressing. The final powder was then pressed into disks using a uniaxially press device at a pressure of 350 bar and within a stainless-steel mold. The

disks were heat-treated in alumina crucibles inside a furnace up to a temperature of 1300°C and finally cooled naturally. The resulting fabricated membranes were utilized for electrofiltration testing.

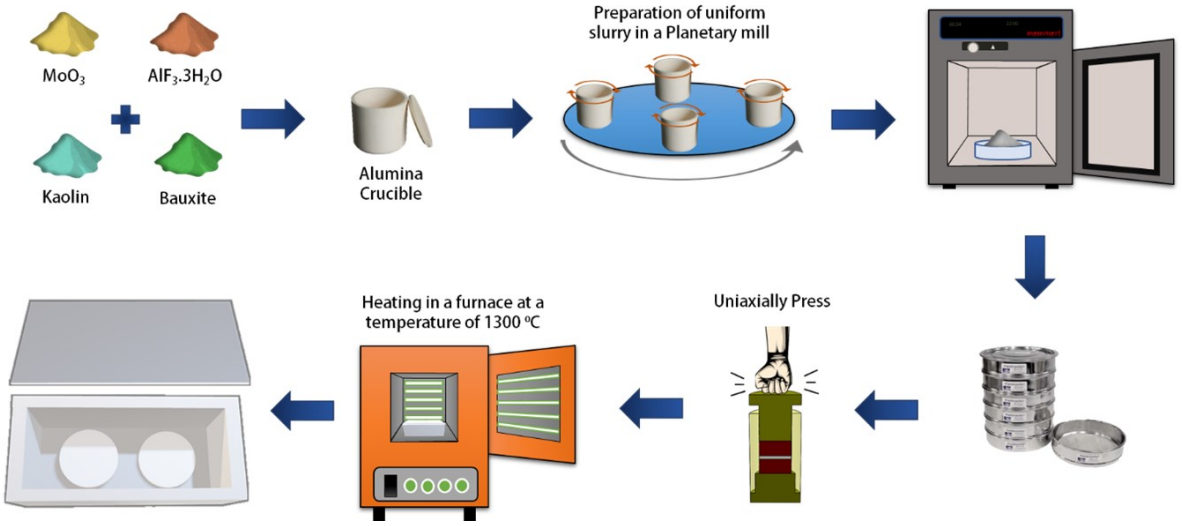

Fig. 1. Schematic of materials and methods used for secondary mullite ceramic membrane synthesis

2.2. Membrane characterization

Various tests were conducted to evaluate the nature and structure of the fabricated membranes, including:

- XRD (X-Ray Diffraction): Performed using an X'Pert MP device (Philips, Netherlands) in the angular range of 4 to 90 degrees.
- SEM (Scanning Electron Microscopy): Conducted using a TESCAN VEGA device (Czech Republic).
- Apparent Porosity Analysis: Carried out using the ASTM-C20 standard method.
- Mercury Intrusion Porosimetry: Performed using a device from Thermo Finnigan (Germany).
- Dimensional Measurement: Conducted using a digital caliper (Mitutoyo, Japan) with an accuracy of 0.01 mm.
- Biaxial Flexural Strength: Performed following the ISO 6872 standard method.

2.3. Filtration experiments

2.3.1. Feed solution preparation and characterization

Crude oil was used to synthesis an oil emulsion, and its specifications are provided in Table 1. A mixture of crude oil and distilled water was subjected to ultrasonic bath treatment at a temperature of 50°C for 1 hour to ensure complete mixing. Fresh feed was used for each test. Subsequently, the obtained emulsion was diluted with distilled water using a laboratory homogenizer at a speed of 2000 rpm to achieve a concentration of 500 mg/L. Sodium sulfate (Na_2SO_4) was used to investigate the effect of salt presence in the oily water emulsion. Salt

concentrations of 0, 1, and 10 mM were examined to assess the impact of salt on the filtration process.

The oily water emulsion was analyzed using Dynamic Light Scattering (DLS) with a Zetasizer Nano ZEN 3600 instrument from Malvern, England, to determine the droplet size distribution and zeta potential. Additionally, the dispersed particle images in water were examined using an optical microscope. The electrical conductivity of the oil emulsion was measured using a GLP32 Crison conductivity meter, Spain, as the presence of salt is one of the influential parameters in the electrofiltration process.

Table 1. materials used for synthesis of crude oil in water emulsion

No.	Material name	Chemical formula	Model	Source
1	Crude oil	$C_{144}H_{141}N_3S_2O_3$	-	Siahmakan, Iran
2	Sodium sulfate	Na_2SO_4	> 99%	Dr.Mojallali Industrial Chemical Complex Company, Iran

2.3.2. Filtration procedure

An oily water emulsion was prepared at varying input pressures (1, 2, and 3 bar) to study the performance of the secondary mullite ceramic membrane in separating oily water emulsions. Fresh membranes were used for each test conducted. The permeate flux (F) in $L/m^2.h$ (LMH) was calculated using the following formula:

$$F = \frac{\mathrm{V}}{\mathrm{A} \times \mathrm{t}} \quad (1)$$

Where V is the volume of permeated water (L), A is the active area of the membrane sample (m^2), and t is the time (h).

The amount of oil present in the permeate was measured using a UV-visible spectrophotometer (OPTIZEN 3220UV, South Korea). The synthesized oily water emulsion exhibited the highest absorption intensity at a wavelength of 220 nm. Based on the UV-visible absorption wavelength spectrum obtained for the desired effluent, the maximum absorption was observed at a wavelength of 220 nm. No change in the wavelength at which maximum absorption occurred was observed with varying oil concentrations in the effluent. Therefore, this wavelength was chosen to determine the oil concentration in the permeate. The correlation coefficient (R^2) of the calibration curve for the effluent was determined to be 0.9985, indicating the high accuracy of the absorption method for determining oil concentrations in the permeate flow. The concentration of the unknown sample was determined using the following relationship. The removal percentage is defined by concentration in the feed (C_f) and the concentration of the same sample in the permeate (C_p) as follows:

$$R = \left(1 - \left(\frac{C_p}{C_f}\right)\right) \times 100 \quad (2)$$

Separation performance tests of the membranes were also conducted to examine the effect of cross-flow velocity at a constant pressure for specific volumetric flow rates of 20 L/h and 40 L/h. Additionally, the temperature was maintained at 25°C throughout the test duration using a constant water bath chamber. During the first 20 minutes of the test, the weight of the permeate was recorded every minute, and thereafter, every 5 minutes. Each test was conducted

for 60 minutes. To maintain the stability of the feed concentration, the permeate samples were returned to the feed container every 10 minutes.

2.3.3. Model analysis for membrane fouling

Modeling the permeate flux reduction provides a better understanding of membrane fouling mechanisms. One of the most successful models used to interpret fouling mechanisms under constant pressure is the Hermia model. According to the Hermia model, which is described in more detail in the available reference (Hermia, 1982), membrane fouling can be classified into four types: complete blocking, intermediate blocking, cake filtration, and standard blocking. The analysis of membrane fouling was performed using the Hermia model for the secondary mullite ceramic membrane.

2.3.4. Backwash

Backwashing with distilled water was employed to investigate membrane fouling. In this regard, the impact of backwashing on restoring the membrane to its initial state was examined. Each backwashing cycle lasted for 15 minutes, followed by a 60-minute assessment of the membrane performance in oily water emulsion filtration.

2.3.5. Electrofiltration procedure

Fig. 2 illustrates the complete electrofiltration system used, which allows for adjusting flow rate, pressure, DC voltage, and membrane backwashing.

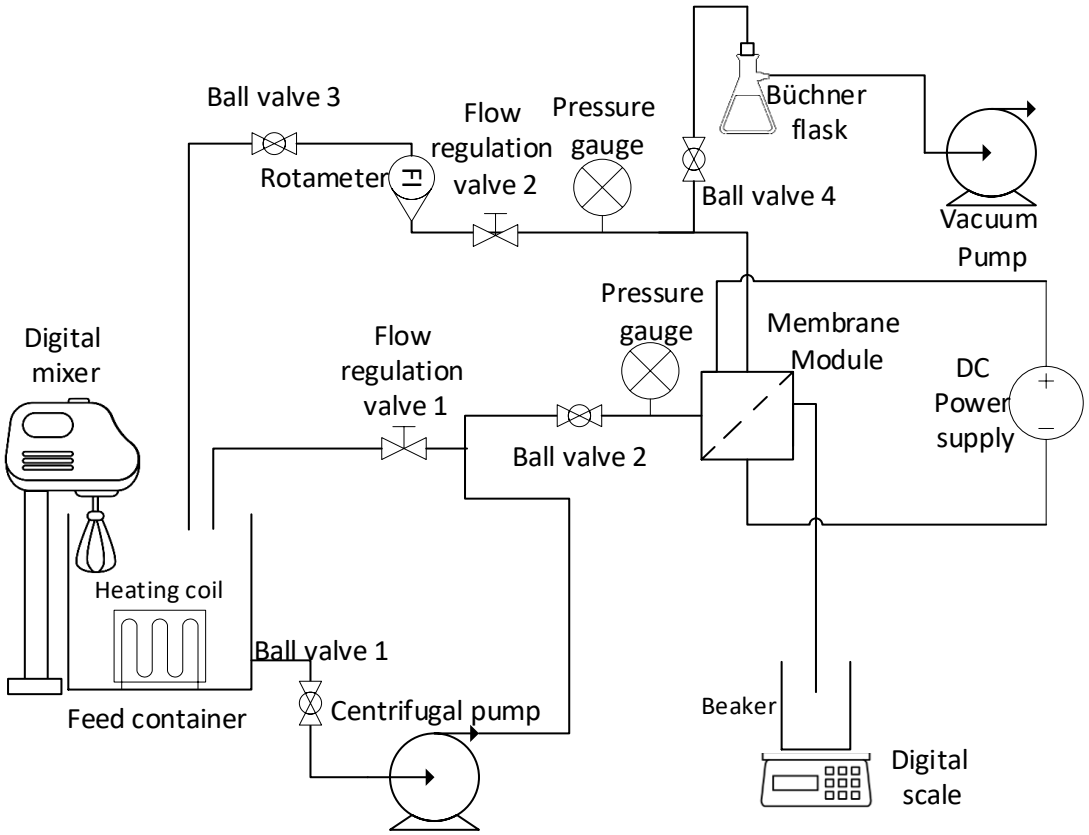

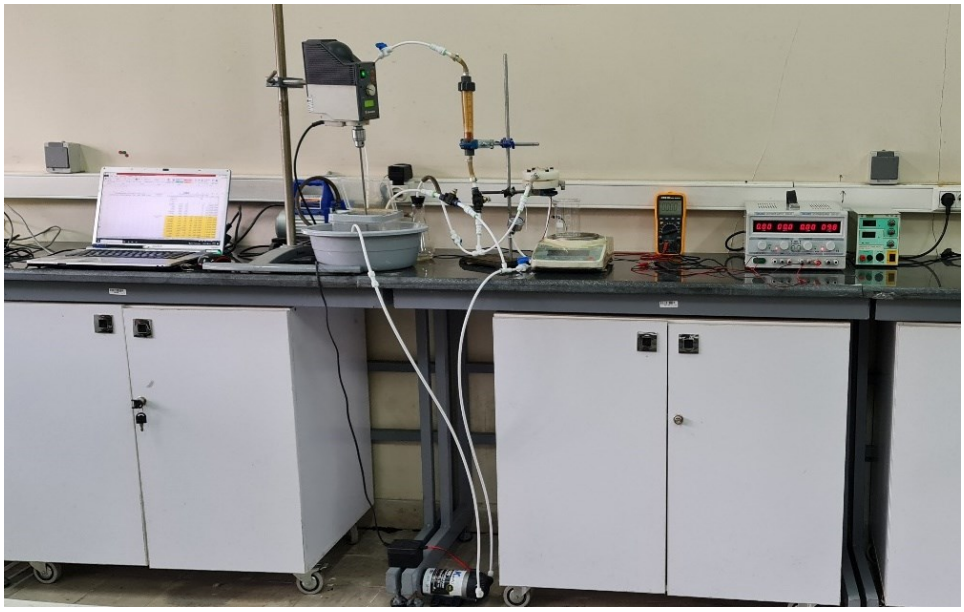

Fig. 2. The schematic diagram and image of the membrane system used for conducting performance tests of the membranes in the electrofiltration and backwashing processes.

In the critical electric field, the variation of permeate flux remains nearly constant with increasing electric voltage. Operating at higher electric field intensities is not economically viable. To determine the critical electric current, salt-free feed was employed. Initially, the permeate flux without electric field was measured under constant pressure, flow rate, and temperature conditions. Then, a series of voltage steps (5 V) was applied to reach E_{crit}. The permeate flux refers to its steady-state value after 60 minutes of system operation. The following empirical formula was used to calculate E_{crit} (Geng and Chen, 2016):

$$E_{crit} = 0.278 \times \frac{J}{\mu_p} \quad (3)$$

where J (LMH) is the pure water flux under similar operating conditions to the oil and water emulsion filtration test, and μ_p is the electrophoretic mobility of oil particles (in μm/s)/(V/cm).

To determine μ_p, an empirical method was employed. In this regard, the movement of oil particles in the oily water emulsion under an electric field intensity of 1 V/cm was examined using an optical microscope, and the displacement of these particles was recorded at specific time intervals. Subsequently, the electrophoretic mobility was calculated using the following formula (Huotari et al., 1999a):

$$\mu_p = \frac{V}{E} \quad (4)$$

where V (μm/s) is the velocity and E (V/cm) is the electric field intensity.

It should be noted that after each experiment, the system was washed with a 0.1% (w/v) NaOH solution and a 0.1% (v/v) nitric acid solution at a temperature of 40°C for 1 hour. Then, the system was rinsed with distilled water for 1 hour. Additionally, to ensure the reproducibility of the experiments, the permeate flux of distilled water was measured after each washing (Chiu and Garcia Garcia, 2011). Using the aforementioned washing method, the changes in permeate flux of the washed membranes were found to be very negligible (less than 1%).

In this study, a process consisting of 9 consecutive stages was designed to investigate the combined effect of filtration, electrofiltration, and backwashing in order to achieve higher separation performance and lower fouling for the synthesized membranes. For each test under different conditions, the system operated without electric field for 15 minutes initially. Then, the system was subjected to electric field for 15 minutes. The field was then interrupted for another 15 minutes, and finally, in the fourth step, the electric field was applied again for 15 minutes. The membrane was backwashed using the provided backwashing method, and the previous four stages were repeated. For electrophoresis examination, salt-free feed, which represents the lowest level of electrical conductivity, was utilized. Feeds with two different electrical conductivities were employed to investigate the effect of presence of salt on membrane performance in the electrofiltration process. Pressure, flow rate, and feed temperature were kept constant throughout all experiments. Additionally, for each new test under different conditions, a fresh membrane was used.

2.4. Energy consumption

The total energy consumption per unit volume of permeate flow at critical flux (E_{tot}) can be calculated in kWh/m^3 using the following equation (Chiu and Garcia Garcia, 2011):

$$E_{tot} = \frac{P_p + P_e}{V_{perm}} = \frac{P_L Q}{J_{crit} S} + \frac{VI}{J_{crit} S} \quad (5)$$

Where P_p, P_e, V_{perm}, P_L, Q, V, I, J_{crit}, and S represent the hydraulic power loss (W), electrical power (W), volume of permeate flow (m^3), pressure difference (Pa), flow rate (m^3/s), applied voltage (V), electric current (A), critical flux through the membrane (m/s), and membrane surface area (m^2), respectively (Chiu and Garcia Garcia, 2011).

It should be noted that the reported results for all experiments are the average of three repetitions of that experiment.

3. Results and discussion

3.1. Membrane characterization

The XRD analysis, pore size distribution, Photograph, and SEM images of the synthesized membrane are presented in Fig. 3. The RIR analysis of the XRD pattern indicates that this membrane has a secondary phase content of 95.4%. The SEM images reveal a highly interconnected needle-like structure with good resistance against shrinkage. The pore size distribution of the membrane, shown in Fig. 3(b), exhibits a single peak and narrow distribution. With an average pore size of 775 nm, the membrane forms a network of needle-like crystallites and exhibits low membrane shrinkage. The radial shrinkage obtained for this membrane is 2.23%. Furthermore, the apparent porosity and biaxial flexural strength of the membrane are 50.37% and 75.21 MPa, respectively.

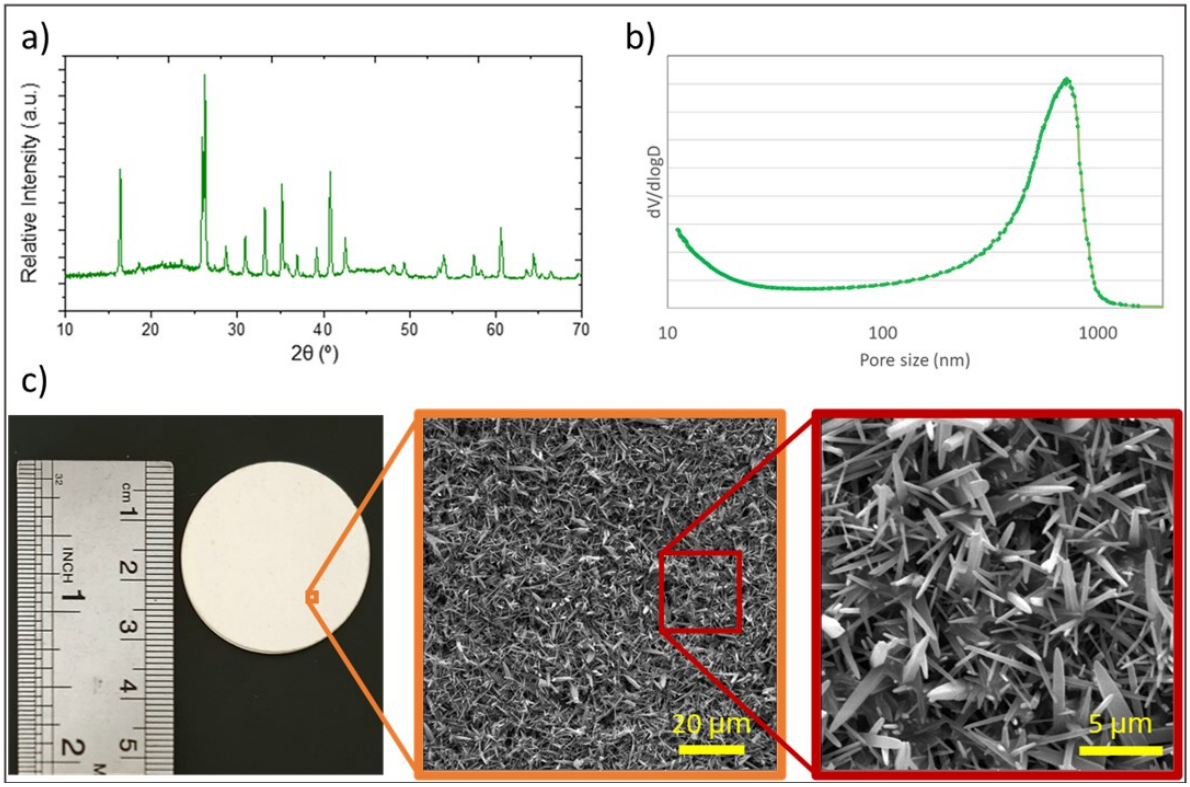

Fig. 3. a) XRD analysis, b) Pore size distribution, and c) Photograph and SEM images of the synthesized secondary mullite ceramic membrane.

3.2. Feed solution characterization

Analysis was performed on the prepared feed samples using the method described in Section 2.3.1, one hour after sample preparations.

The particle size distribution of oil particles in the emulsion is shown in the Fig. 4. The average oil particle size is 1.3 µm, which is larger than the average pore size of the synthesized membranes. This indicates that the synthesized membranes have the ability to reject oil particles. Additionally, optical microscopy images of dispersed oil particles examined using an optical microscope are presented in the same figure.

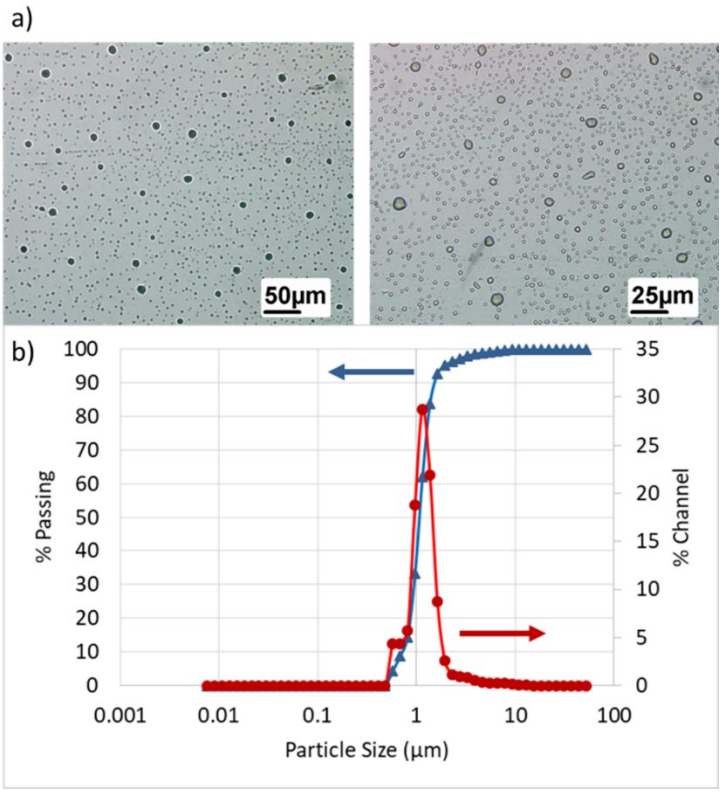

Fig. 4. a) Optical microscopy images, and b) Particle size distribution of the synthesized oily water emulsion

The zeta potentials of oil particles in deionized water, 1 mM, and 10 mM Na_2SO_4 solutions were -46.8, -41.2, and -26.1 mV, respectively. These values indicate that in electrofiltration, when the membrane is positioned between two electrodes, the anode should be placed on the inlet flow side. Furthermore, the absolute reduction in the zeta potential of oil particles in water increases with the addition of Na_2SO_4 due to enhanced adsorption on the particle surfaces. This means that by adding the salt, the concentration of electrolyte ions in the solution increases. As a result, a higher electric charge is formed on the particles surface. The positive charges of the salt and the negative charges from the particles interact in the solution and reach an average equilibrium on the particles surface. This enhanced adsorption on the particles surface leads to a reduction in the zeta potential of the solution. The reason is that particles with higher electric charge have a larger electric double-layer thickness. In other words, the distance between positive and negative charges on the particle surface decreases, resulting in a decrease in the zeta potential of the solution (Elzo et al., 1998). Additionally, the experimental value of electrophoretic mobility was obtained as 3.96 (µm/s)/(V/cm). Furthermore, using an electrical conductivity meter, the electrical conductivity of the feed increased from 3.73 µS/cm to 241.00 µS/cm and 1922.00 µS/cm as the concentration of Na_2SO_4 increased from 0 mM to 1 mM and 10 mM, respectively.

3.3. Filtration experiments

3.3.1. Effect of pressure

To explore the isolated impact of pressure on separation performance, the flow velocity was deliberately set to zero. As shown in Fig. 5(a), higher pressure resulted in higher initial permeate flux in all membranes due to stronger driving force. However, with increasing pressure, the nonlinearity of changes in permeate flux over time also increased, which can be

attributed to increased crude oil droplet compression on the membrane surface. For example, although the initial permeate flux was higher at 3 bar compared to 2 bar, they tended to converge over time. Fig. 5(b) demonstrates a partial increase in oil rejection percentage with increasing pressure. Increasing pressure led to the formation of a thicker cake layer, which created a greater barrier for oil droplets to pass through membrane pores. Within the tested pressure range, oil rejection ranged between 94.7% and 95.7% for a 500 ppm solution. The final permeate flux at 2 bar was 534 L/m²·h (LMH), which is a significant value compared to the permeate flux of a secondary mullite membrane synthesized by Rashad et al.(Rashad et al., 2021) under similar conditions, which was 336 LMH.

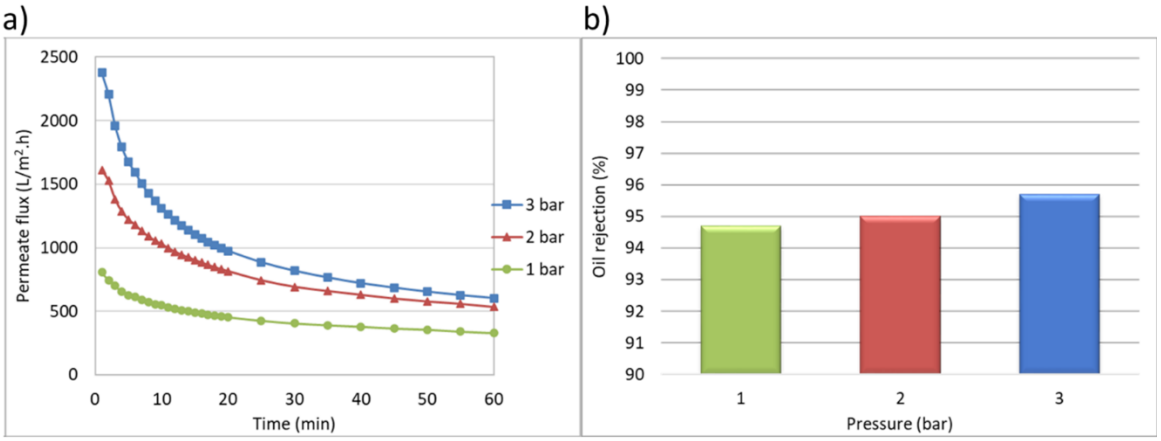

Fig. 5. a) Separation of oily water emulsion in a dead-end configuration under pressures of 1, 2, and 3 bar. b) Final oil rejection percentages (%) at different pressures.

Considering that increasing pressure leads to an increase in pump power consumption, selecting very high pressures would not be economically viable. The optimal pressure should be chosen in a way that both membrane flux and oil rejection factors are acceptable. Since high pressure differentials result in the accumulation of a gel layer on the membrane surface and a decrease in the permeate flux over time, applying excessively high pressure as the driving force incurs high costs and reduces the lifespan of membrane performance. Therefore, based on the conducted experiments, a pressure of 2 bar was selected as the preferred pressure for further investigations.

3.3.2. Effect of cross-flow velocity

To investigate the effect of crossflow velocity on the performance of a ceramic membrane separation at a constant pressure of 2 bars and a constant temperature of 25°C, the crossflow velocity was varied. The performance of the secondary membrane was examined at flow velocities equivalent to volumetric flow rates of 20 and 40 L/h, corresponding to average velocities of 0.727 and 1.454 m/s, respectively.

Fig. 6 illustrates the variations in permeate flux over time and the final oil rejection percentage at different crossflow velocities. The crossflow velocity of zero, or microfiltration under dead-end condition, has the lowest transmembrane flux and the highest membrane fouling. With increasing velocity, a decrease in fouling can be observed by the decreasing slope of the permeate flux curve over time. The decrease in oil rejection percentage with increasing crossflow velocity is attributed to turbulent flows that prevent the formation of a cake layer,

which acts as a barrier for impurity passage, due to the removal of materials that can deposit on the membrane surface. Additionally, due to increased mass transfer, the possibility of oil particle passage increases, resulting in reduced membrane rejection and separation percentage.

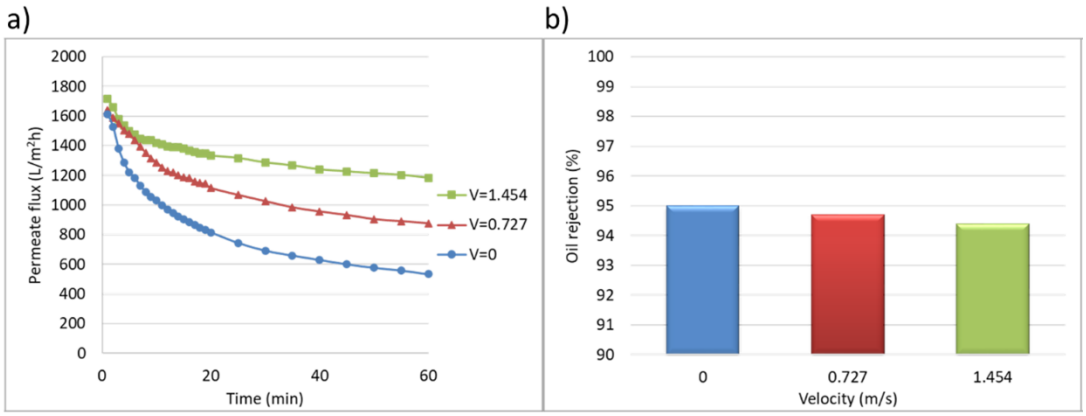

Fig. 6. a) Separation of oily water emulsion at a constant pressure of 2 bar and three different velocities: 0, 0.727 m/s, and 1.454 m/s. b) Final oil rejection percentage (%) at different velocities.

The selected crossflow velocity in this stage is used in the subsequent stages as well. In the electrofiltration process, due to the accumulation of pollutant particles (in this case, crude oil particles) on the anode electrode, there is no need for high flow velocity to minimize cake formation. In fact, increasing the velocity in electrofiltration process is detrimental and causes the pollutants to flow towards the membrane (Huotari, 2000). Taking into account the aforementioned factors, as well as the permeate flux, separation percentage, and energy consumption, the selected crossflow velocity for further tests was 0.727 m/s.

3.3.3. Model analysis for membrane fouling

Fig.7 illustrates the results of the model analysis for membrane fouling for oily water emulsion at a pressure of 2 bar and a flow velocity of 0.727 m/s.

For the treatment of oily water emulsion, the values of R^2 for complete blocking, intermediate blocking, cake filtration, and standard blocking models are 0.89, 0.94, 0.97, and 0.92, respectively. A higher value of R^2 indicates a better fit of the model. Therefore, the cake filtration and intermediate fouling models exhibit the best agreement with the permeate flux reduction data. In these mechanisms, particles accumulate on the membrane surface and form a cake layer. These types of fouling are reversible.

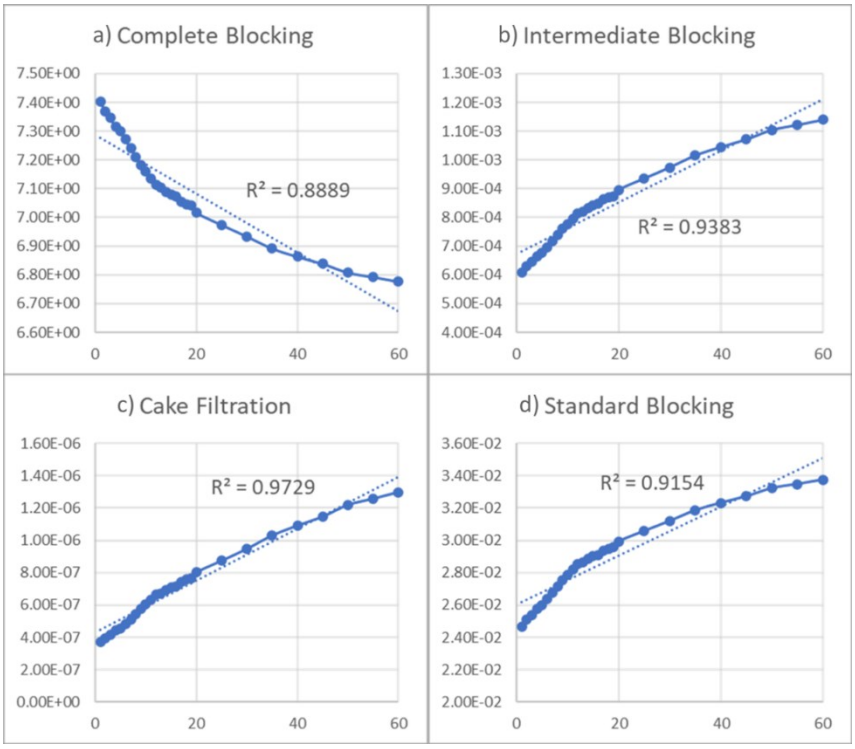

Fig. 7. Reduction of permeate flux over time for oily water emulsion at different fouling models

3.3.4. Effect of backwash

Fouling exists in all pressured membrane systems. Fouling reduces the permeate flux and shortens the useful life of membranes. Therefore, membrane cleaning is an essential and inseparable part of most practical membrane processes and should be performed regularly. Fouling can be generally categorized into two types: reversible fouling and irreversible fouling. Permeate flux can easily be recovered after cleaning the membrane under reversible fouling conditions, while irreversible fouling leads to irreversible loss of permeate flux. In this study, backwashing with distilled water was used to investigate both reversible and irreversible fouling. The tested membrane, subjected to a pressure of 2 bar and a flow velocity of 0.727 m/s during a 60-minute test, underwent a 15-minute backwashing with distilled water and then was subjected to another 60-minute test for oily water filtration under the same initial conditions. The graphs in Fig. 8 depict the membrane performance before and after the backwashing. As evident, the backwashing partially restored the membrane performance to its initial state but still had some deviation. Additionally, the performance trend of the membrane before and after backwashing is almost the same, with the difference being that the range of permeate flux variations after backwashing is smaller than the range before it.

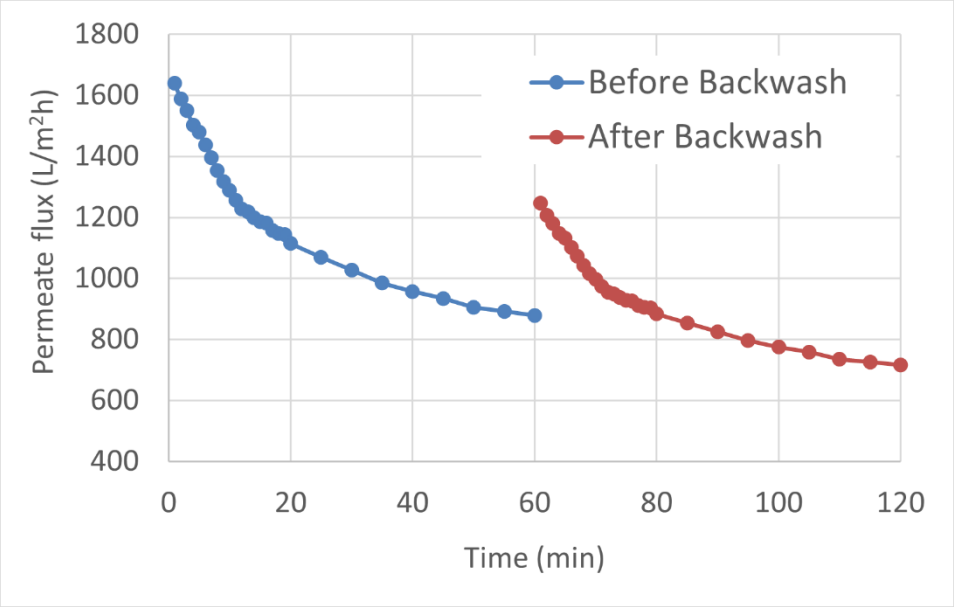

Fig. 8. Membrane performance in oily water filtration at a pressure of 2 bar and a flow velocity of 0.727 m/s, before and after a 15-minute backwashing.

As shown in Fig. 8, the initial permeate flux was recovered to approximately 76% of the initial flux after a 15-minute backwashing. However, this incomplete recovery of permeate flux with backwashing after one operating cycle necessitates the use of other methods to reduce fouling and increase membrane lifespan.

3.4. Electrofiltration

3.4.1. E_{crit}

At a pressure of 2 bar and a flow velocity of 0.727 m/s, the synthesized membrane was subjected to different electric field intensities to determine its E_{crit} experimentally. The feed used in these experiments was an oily water emulsion without electrolytes. The graph illustrating the changes in permeate flux as a function of voltage when the membrane is placed between two electrodes is shown in Fig. 9.

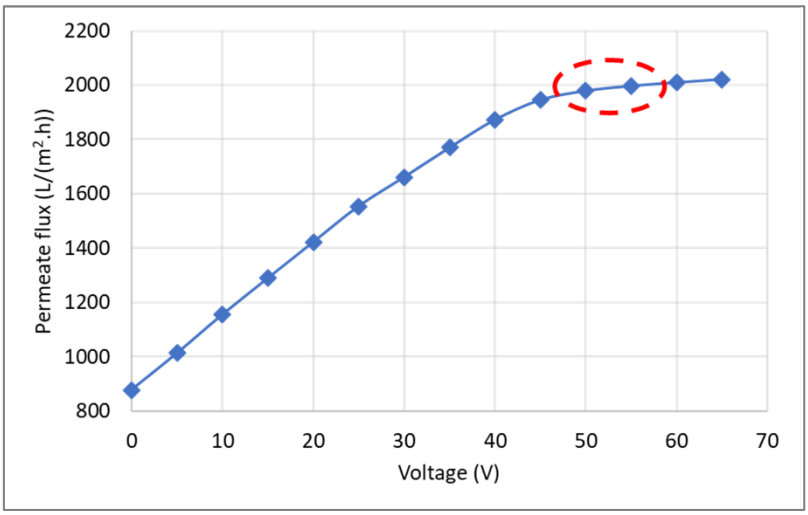

Fig. 9: Variation of permeate flux with changing voltage for oily water emulsion. E_{crit} is indicated by a red ellipse on the graph.

As the voltage increases, the permeate flux also increases. Since the oil particles in the feed have a negative charge, increasing the electric field intensity results in a higher electrostatic force acting on the particles. When this force overcomes the other forces acting on the particles that contribute to fouling, it causes them to move away from the membrane surface. As a result, fouling caused by these particles is reduced, and the flux increases. Additionally, according to the smoluchowski equation, the electroosmotic velocity also increases with the electric field intensity. Therefore, increasing the electric field intensity leads to an enhancement of both electrophoresis and electroosmosis phenomena. However, at a certain electric field intensity (E_{crit}), the slope of the flux variation decreases. E_{crit} arises due to the limitation in the number of particles that the electric field can displace. According to Fig. 9, the critical electric field intensity in the experimental conditions falls within the range of 50 to 55 V. When the electric field intensity exceeds the critical range, further increases, although resulting in a linear increase in permeate flux, have a minimal effect due to the low slope of the flux variations. Therefore, operating the system at electric field intensities higher than E_{crit} is not economical.

E_{crit} can also be theoretically calculated using Equation (3). The flux of distilled water at a pressure of 2 bar and a velocity of 0.727 m/s increases to 83.1975 LMH with increasing mass transfer velocity. Thus, considering the electrophoretic mobility of oil particles at 3.96 (μm/s)/(V/cm), E_{crit} will be at 55.5 V. The obtained value for E_{crit} from both experimental and theoretical approaches is close to each other and confirms one another. Hence, to investigate the effect of electric field on the performance of the synthesized membrane, voltages of 15, 25, 45, and 65 V were utilized. Based on the measured potential, indicating the negative charge of the particle, and to enhance the membrane performance, the anode was placed on the feed side, while the cathode was placed on the permeate side.

3.4.2. Effect of electrical field strength

Fig. 10(a) illustrates the variations in normalized permeate flux over time at different voltages for the electrolyte-free feed. According to the figure, the relative permeate flux of the membrane in all experiments decreases during the initial 15 minutes, which corresponds to the filtration process. This reduction is due to the rapid accumulation of oil particles on the membrane surface and the increasing fouling. In the second 15 minutes, when electrofiltration is employed, the relative permeate flux increases with the applied voltage, leading to an enhancement of the electrophoresis phenomenon and the removal of oil particles from the surface. At the minute 30, for voltages of 15, 25, 45, and 65 V, the J/J_0 ratio is 76%, 84%, 94%, and 128%, respectively. Due to the flow velocity in the feed direction and the generation of turbulence, the flow mixes in the feed direction. This phenomenon causes the previously separated particles to come close to each other again. In the relative permeate flux graph at 15 V, a slight decrease is observed, which is attributed to this phenomenon. As the voltage increases and the electrophoresis effect becomes dominant, the impact of this decrease diminishes, which is confirmed by the graphs. At 65 V, which is higher than the critical voltage, the maximum electrophoresis effect is present. The permeate flux is slightly higher than the initial flux, which occurs due to electroosmosis in the presence of oil particles. In the absence

of cake layer and concentration polarization, the electroosmosis phenomenon occurs. Furthermore, the current at this voltage was 1.61 mA.

In the third 15-minute interval, where only filtration is present again, the membrane permeate flux decreases after discontinuing the application of voltage but is still higher than the state without electrical field. This indicates that applying voltage to the membrane is beneficial for improving the permeate flux. When $E<E_{crit}$, oil particles are not completely removed during the electrofiltration process. Therefore, a weak cake layer exists on the membrane surface, which protects the membrane from severe fouling. At the beginning of the third 15-minute interval, for 65 V and when $E>E_{crit}$, the membrane permeate flux decreases significantly due to the absence of deposition and accumulation of contaminants, reaching its initial value.

In the fourth 15-minute interval, with the reapplication of the electric field, the membrane permeate flux increases in all voltages. However, the relative fluxes are lower than the values in the second 15-minute interval. This is because electrophoresis has difficulty reducing the accumulation of oil particles inside the membrane pores during the electrofiltration process. Therefore, over time, the permeate flux of the membrane decreases.

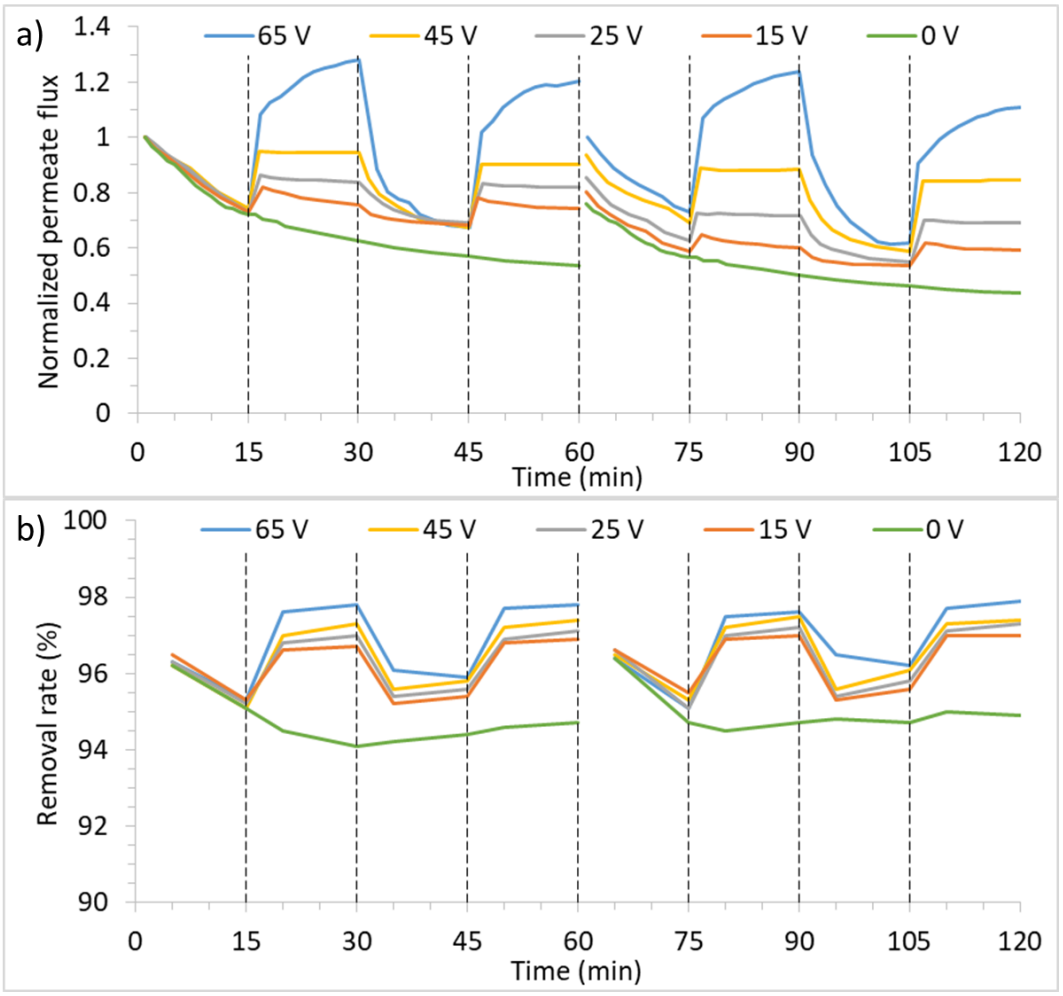

Fig. 10. a) Normalized permeate flux over time, b) Removal rate over time for the synthesized membrane, before and after backwashing at salt concentration of 0 mM, at different voltages

The effect of applying an electric field on the fouling removal rate is shown in Fig. 10(b). Generally, increasing the fouling layer thickness leads to a decrease in permeate flux but improves fouling mitigation. Despite the smaller average pore size of membrane compared to oil droplets, larger pores may allow the passage of some small oil droplets, initially reducing oil removal efficiency. Over time, the clogging of membrane pores by oil particles during filtration leads to pore size reduction and improved fouling mitigation. This trend can be observed in the removal rate graph for the zero-voltage condition. The fouling removal rate at the minute 60 without electric field is 94.7%. Applying an electric field and particle detachment from the membrane surface showed improved fouling mitigation. At minute 30, fouling removal rate percentages of 96.7%, 97%, 97.3%, and 97.8% were achieved for voltages of 15, 25, 45, and 65 V, respectively. Upon turning off the electric field, due to the increased cake layer thickness and the clean membrane surface, a decrease in fouling removal rate followed by an increase was observed in the third 15-minute interval. In the case of 65 V, due to the complete cleanliness of the membrane surface, the fouling removal rate variations follow a similar trend to the first 15-minute interval. By reapplying the electric filed in the fourth stage, fouling removal rate increased, but not as much as in the second 15-minute interval.

Due to the reduction in pore size caused by the presence of oil particles inside the pores and the ineffectiveness of backwashing on them, the fouling removal rate percentage is slightly higher (95% at minute 60) for the zero electric field condition. However, for the case of applying voltage, there is no significant difference observed. The application of force on oil particles by the electric field and their detachment from the membrane surface reduce their presence on the membrane and result in a consistent fouling mitigation percentage after backwashing.

3.4.3. Effect of feed solution electrical conductivity

The wastewaters discharged from crude oil desalination units contain significant amounts of salt. There are different opinions regarding the effect of salt on membrane permeance and fouling percentage. Salt concentration can play a determining role in membrane performance. As the salt concentration increases, the thickness of the electrical double layer decreases, resulting in stronger electrostatic repulsion and a tendency for oil particles to aggregate and foul the membrane. Additionally, increasing salt concentration leads to an increase in the viscosity of the wastewater. On the other hand, the formation of salt crystals due to salt concentration polarization on the membrane surface causes membrane pores to be blocked, resulting in an increase in fouling percentage. However, the presence of ions on the membrane surface can cause the detachment of charged particles from the membrane surface and reduce fouling. Furthermore, by creating an ion potential difference across the membrane, it can increase permeance due to the electroosmosis phenomenon.

Based on the performance graphs for the zero electrical field in Fig. 11(a) and Fig. 11(c), the explained different effects in the previous paragraph can be observed in the presence of salt. At a concentration of 1 mM, the membrane performance remains unaffected, but at a higher concentration of 10 mM, a decrease in membrane performance was observed due to increased

concentration polarization and a reduction in the thickness of the electrical double layer of oil particles. It is also worth mentioning that the feed flow velocity has a significant impact on this decrease in performance, and severe fouling was not occurred. The permeate flux ratio at minute 60 in a concentration of 10 mM has a reduction of 5% compared to lower concentrations. After backwashing at a concentration of 10 mM, a lower recovery rate compared to lower concentrations was also observed. The recovery rates were 74% and 70% for 1 mM and 10 mM, respectively.

The effect of changing salt concentration on the electrofiltration process is also evident in the graphs of Fig. 11(a) and Fig. 11(c). At 1 mM, an improvement in membrane performance was observed with increasing voltage. At minute 30, for the voltages of 15, 25, 45, and 65 V, J/J_0 ratios were 74%, 89%, 96%, and 150%, respectively. The increase in electroosmosis due to the presence of salt may be the reason for the increase in these ratios. Additionally, due to the presence of salt, an increase in voltage results in an increase in electrical current, which causes reactions at the anode surface and bubble formation. The reduction in relative flux during the second stage at different voltages indicates a decrease in the influence of the electric field due to bubble formation at the anode surface and in the feed stream, as well as a decrease in zeta potential. This reduction is more pronounced at higher voltages. The highest relative flux ratio at 65 V is 158%, and after that, it reaches 150% at minute 30. The flow velocity, in addition to particle displacement, also causes bubble displacement and their approach to the membrane surface. As a result, the application of an electric field does not significantly improve the filtration. In 10 mM salt concentration, due to the increase in electrical current with increasing salt concentration (from 103.6 mA at 1 mM to 830 mA at 10 mM), more bubbles are formed on the anode surface, leading to a decrease in the electrophoresis phenomenon. Additionally, in this concentration, zeta potential has also decreased further. At minute 30, for voltages of 15, 25, 45, and 65 V, J/J_0 ratios were 67%, 71%, 76%, and 77% respectively, showing a decrease compared to1 mM. Therefore, the membrane flux is determined by the effects of bubbles and electroosmosis, resulting in irregular variations in membrane flux between 1 mM and 10 mM.

The membrane performance after backwashing at different salt concentrations was also examined. Generally, the recovery improved with increasing voltage. After backwashing, in the zero-voltage state, a recovery of 74%, and at 65 V, a recovery of 99% were observed. The flux recovery values for these conditions at 10 mM are lower due to the presence of salt and increased irreversible fouling. These values are 70% and 83% for voltages of zero and 65 V, respectively.

Fig. 11(b) and Fig. 11(d) illustrate the changes in removal rate percentage with time and voltage for salt concentrations of 1 and 10 mM. With an increase in salt concentration, due to increased fouling, an improvement in fouling percentage was achieved, from 94.8% at 1 mM to 95% at 10 mM. Additionally, removal rate percentages at voltages of 15, 25, 45, and 65 V at minute 30, for 1 mM, are 96.2%, 97.3%, 97.5%, and 98.1%, respectively, and for 10 mM, they are 95.6%, 95.8%, 96.1%, and 96.4%, respectively. The presence of bubbles and the reduction in electrophoretic effects are the reasons for the decrease in fouling percentage at 10 mM. By interrupting the voltage at 1 mM, the oil particle removal rate initially decreases and then

slightly increases in the graphs for 15, 25, 45, and 65 V. The reason is that in lower electrolyte concentrations, due to the lesser effect of bubbles formed on the anode and feed side, contaminants can be easily expelled from the membrane surface, and after voltage interruption, contaminants gradually reattach to the membrane surface. In contrast, at 10 mM, after current interruption, the fouling rate increases with increasing voltage, which confirms the formation of bubbles due to increased electric current, reduction in electrophoretic effects, and increased fouling. As evident, the membrane performance in terms of permeate flux and fouling percentage is better when voltage is applied at 1 mM compared to 10 mM. Generally, the fouling percentages after backwashing at 10 mM are higher than at 1 mM. This higher value indicates a higher irreversible fouling at higher salt concentrations, even in the presence of applied voltage.

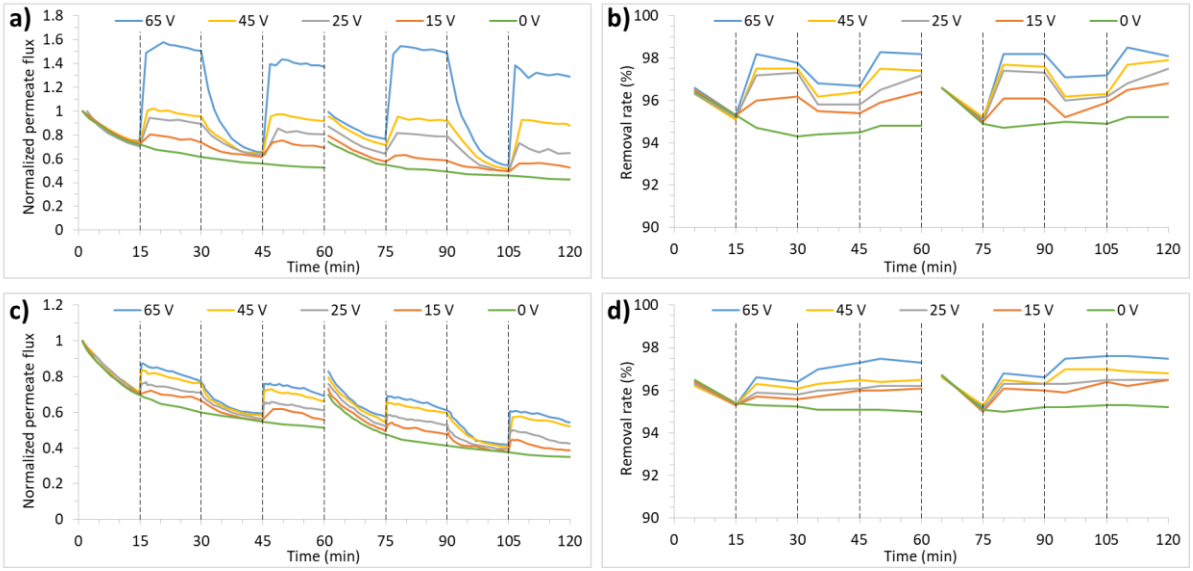

Fig. 11. a) Normalized permeate flux over time at a 1 mM salt concentration, b) Removal rate over time at a 1 mM salt concentration, c) Normalized permeate flux over time at a 10 mM salt concentration, d) Removal rate over time at a 10 mM salt concentration, before and after backwashing, at different voltages

3.5. Energy consumption

Fig. 12 shows the energy consumption graphs in terms of applied voltages for solutions with different electrical conductivities in the electrofiltration process. At low conductivity, the energy consumption in the applied voltage range in this study decreases. In the salt-free condition, the energy consumption has decreased from 3.88 kWh/m³ in the no-voltage condition to 2.71 kWh/m³ at 65 V. However, as the conductivity increases, there is a minimum value for energy consumption where the electric field intensity is optimal. In the graph for 1 mM, there is no significant increase in energy consumption up to 25 V voltage, but after that, there is a noticeable increase. As observed, with further increase in the electrical conductivity of the solution, the energy consumption increases significantly, and it will not be economical to use it.

The post backwashing graphs in Fig. 12 for different concentrations indicate that the specific energy consumption trend with respect to voltage in these graphs is similar to the pre backwashing state. However, these graphs for 0 mM and 1 mM concentrations are closer to

their pre backwashing graphs compared to the 10 mM concentration. This once again confirms that at higher salt concentrations, there is greater fouling and less effect of the electric field. Additionally, since the pre and post backwashing graphs are closer to each other at lower salt concentrations, the membrane process design with these concentrations encounters less error and provides results with lower uncertainty.

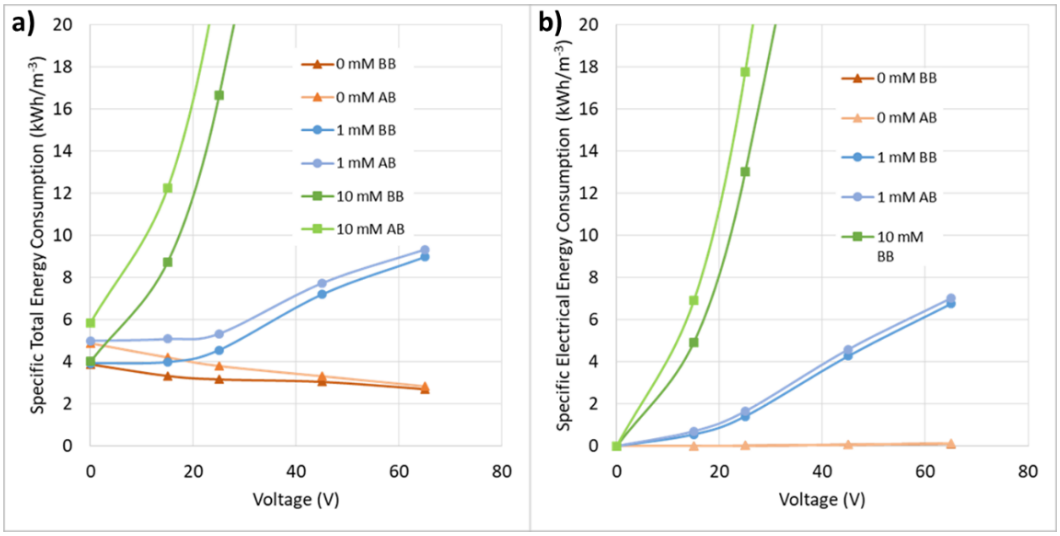

Fig. 12. Energy consumption as a function of voltage for different salt concentrations before (BB) and after (AB) backwashing of the membranes: a) Electrical energy consumption, b) Total energy consumption

4. Conclusions

In conclusion, this study investigated the potential of ceramic membrane-based electrofiltration for the treatment of oily water. The synthesized secondary mullite membrane exhibited favorable characteristics, including high permeate flux (534 LMH) and biaxial flexural strength (75.21 MPa), while maintaining cost-effectiveness. Optimization of operational parameters, such as pressure (2 bar) and cross-flow velocity (0.727 m/s), resulted in desirable permeate flux and oil removal rates. Using only filtration, backwashing with distilled water resulted in a 76% recovery of membrane initial performance. The critical electric field intensity (E_{crit}) range of 50 to 55 V was determined, guiding the selection of optimal voltages for electrofiltration and mitigating fouling through various electrokinetic phenomena. Higher salt concentrations were found to increase fouling and reduce electric field effectiveness. Energy consumption analysis revealed reduced energy requirements at low electrical conductivities, reaching 2.71 kWh/m³ at 65 V for the salt-free condition. However, higher electrical conductivity led to increased energy consumption, limiting practical viability. Overall, careful control of operational parameters, particularly voltage, enabled significant improvements in permeate flux, fouling removal rates, and energy efficiency. These findings contribute to the advancement of the designed process for combined filtration, electrofiltration, and backwashing, offering a promising solution for effective and sustainable treatment of oily water using the synthesized mullite whiskers membrane.

References

Abdullayev, A., Avcioglu, C., Fey, T., Hilger, A., Osenberg, M., Manke, I., Henning, L.M., Gurlo, A. and Bekheet, M.F. 2022. Fabrication and characterization of porous mullite ceramics derived from fluoride-assisted Metakaolin-Al(OH)3 annealing for filtration applications. Open Ceramics 9, 100240.

Agana, B.A., Reeve, D. and Orbell, J.D. 2012. The influence of an applied electric field during ceramic ultrafiltration of post-electrodeposition rinse wastewater. Water Research 46(11), 3574-3584.

Ahmed, S.F., Mofijur, M., Nuzhat, S., Chowdhury, A.T., Rafa, N., Uddin, M.A., Inayat, A., Mahlia, T.M.I., Ong, H.C., Chia, W.Y. and Show, P.L. 2021. Recent developments in physical, biological, chemical, and hybrid treatment techniques for removing emerging contaminants from wastewater. Journal of Hazardous Materials 416, 125912.

Akhondi, E., Wicaksana, F. and Fane, A.G. 2014. Evaluation of fouling deposition, fouling reversibility and energy consumption of submerged hollow fiber membrane systems with periodic backwash. Journal of Membrane Science 452, 319-331.

Al-Kaabi, M.A., Zouari, N., Da'na, D.A. and Al-Ghouti, M.A. 2021. Adsorptive batch and biological treatments of produced water: Recent progresses, challenges, and potentials. Journal of Environmental Management 290, 112527.

Campo, R., Giustra, M.G., De Marchis, M., Freni, G. and Di Bella, G. 2017. Characterization and Treatment Proposals of Shipboard Slop Wastewater Contaminated by Hydrocarbons. Water 9(8), 581.

Chen, J.-P., Yang, C.-Z., Zhou, J.-H. and Wang, X.-Y. 2007. Study of the influence of the electric field on membrane flux of a new type of membrane bioreactor. Chemical Engineering Journal 128(2), 177-180.

Chiu, T.Y. 2013. Electrically Assisted Microfiltration of Whey Suspensions using Non-Circular Multichannel Ceramic Membranes. Separation Science and Technology 48(1), 84-92.

Chiu, T.Y. and Garcia Garcia, F.J. 2011. Critical flux enhancement in electrically assisted microfiltration. Separation and Purification Technology 78(1), 62-68.

Coca, J., GutiÉRrez, G. and Benito, J. 2011. Treatment of Oily Wastewater. 1-55.

Davoodbeygi, Y., Askari, M., Salehi, E. and Kheirieh, S. 2023. A review on hybrid membrane-adsorption systems for intensified water and wastewater treatment: Process configurations, separation targets, and materials applied. Journal of Environmental Management 335, 117577.

Dong, Y., Wu, H., Yang, F. and Gray, S. 2022. Cost and efficiency perspectives of ceramic membranes for water treatment. Water Research 220, 118629.

Du, F., Ciaciuch, P., Bohlen, S., Wang, Y., Baune, M. and Thöming, J. 2013. Intensification of cross-flow membrane filtration using dielectrophoresis with a novel electrode configuration. Journal of Membrane Science 448, 256-261.

Du, F., Hawari, A., Baune, M. and Thöming, J. 2009. Dielectrophoretically intensified cross-flow membrane filtration. Journal of Membrane Science 336(1), 71-78.

Elzo, D., Huisman, I., Middelink, E. and Gekas, V. 1998. Charge effects on inorganic membrane performance in a cross-flow microfiltration process. Colloids and Surfaces A: Physicochemical and Engineering Aspects 138(2), 145-159.

Eom, J.-H., Kim, Y.-W., Yun, S.-H. and Song, I.-H. 2014. Low-cost clay-based membranes for oily wastewater treatment. Journal of the Ceramic Society of Japan 122(1429), 788-794.

Fu, M., Liu, J., Dong, X., Zhu, L., Dong, Y. and Hampshire, S. 2019. Waste recycling of coal fly ash for design of highly porous whisker-structured mullite ceramic membranes. Journal of the European Ceramic Society 39(16), 5320-5331.

Geng, P. and Chen, G. 2016. Magnéli Ti4O7 modified ceramic membrane for electrically-assisted filtration with antifouling property. Journal of Membrane Science 498, 302-314.

639 Goh, P.S., Wong, K.C. and Ismail, A.F. 2022. Membrane technology: A versatile tool for saline
640 wastewater treatment and resource recovery. Desalination 521, 115377.
641 Gu, Q., Ng, T.C.A., Bao, Y., Ng, H.Y., Tan, S.C. and Wang, J. 2022. Developing better ceramic
642 membranes for water and wastewater Treatment: Where microstructure integrates with
643 chemistry and functionalities. Chemical Engineering Journal 428, 130456.
644 Guo, H., Li, W. and Ye, F. 2016. Low-cost porous mullite ceramic membrane supports fabricated
645 from kyanite by casting and reaction sintering. Ceramics International 42(4), 4819-4826.
646 Hermia, J. 1982 Constant Pressure Blocking Filtration Laws - Application To Power-law Non-
647 newtonian Fluids.
648 Hu, C., Li, M., Sun, J., Liu, R., Liu, H. and Qu, J. 2019. NOM fouling resistance in response to electric
649 field during electro-ultrafiltration: Significance of molecular polarity and weight. Journal of
650 Colloid and Interface Science 539, 11-18.
651 Huang, J., Wang, Z., Zhang, J., Zhang, X., Ma, J. and Wu, Z. 2015. A novel composite conductive
652 microfiltration membrane and its anti-fouling performance with an external electric field in
653 membrane bioreactors. Scientific Reports 5(1), 9268.
654 Hubadillah, S.K., Othman, M.H.D., Matsuura, T., Rahman, M.A., Harun, Z., Jaafar, J. and Nomura, M.
655 2017. Fabrications and applications of low cost ceramic membrane from kaolin: A
656 comprehensive review. Ceramics International.
657 Huotari, H.M., Huisman, I.H. and Trägårdh, G. 1999a. Electrically enhanced crossflow membrane
658 filtration of oily waste water using the membrane as a cathode. Journal of Membrane
659 Science 156(1), 49-60.
660 Huotari, H.M., Trägårdh, G. and Huisman, I.H. 1999b. Crossflow Membrane Filtration Enhanced by
661 an External DC Electric Field: A Review. Chemical Engineering Research and Design 77(5),
662 461-468.
663 Huotari, H.M.a.N., M. 2000. Electrofiltration in industrial wastewater applications. Transactions of
664 the Filter Society 1, 17-22.
665 Khosravanipour Mostafazadeh, A., Zolfaghari, M. and Drogui, P. 2016. Electrofiltration technique
666 for water and wastewater treatment and bio-products management: A review. Journal of
667 Water Process Engineering 14, 28-40.
668 Kyllönen, H. (2005) Electrically or ultrasonically enhanced membrane filtration of wastewater,
669 Lappeenranta University of Technology Laboratory of Membrane Technology and Technical
670 Polymer Chemistry
671 Lee, H.-H., Weng, Y.-H. and Li, K.-C. 2008. Electro-ultrafiltration study on Aldrich humic substances
672 with different molecular weights. Separation and Purification Technology 63(1), 23-29.
673 Li, C., Sun, W., Lu, Z., Ao, X. and Li, S. 2020. Ceramic nanocomposite membranes and membrane
674 fouling: A review. Water Research 175, 115674.
675 Naseri, M. and Omidkhah, M.R. 2023. Optimizing the fabrication conditions of monolithic mullite
676 whisker membrane from kaolin and bauxite using the Taguchi method. Ceramics
677 International 49(14, Part A), 23612-23626.
678 Nthunya, L.N., Bopape, M.F., Mahlangu, O.T., Mamba, B.B., Van der Bruggen, B., Quist-Jensen, C.A.
679 and Richards, H. 2022. Fouling, performance and cost analysis of membrane-based water
680 desalination technologies: A critical review. Journal of Environmental Management 301,
681 113922.
682 Oussedik, S., Belhocine, D., Grib, H., Lounici, H., Piron, D.L. and Mameri, N. 2000. Enhanced
683 ultrafiltration of bovine serum albumin with pulsed electric field and fluidized activated
684 alumina. Desalination 127(1), 59-68.
685 Rashad, M., Logesh, G., Sabu, U. and Balasubramanian, M. 2021. A novel monolithic mullite
686 microfiltration membrane for oil-in-water emulsion separation. Journal of Membrane
687 Science 620, 118857.

Salahi, A., Gheshlaghi, A., Mohammadi, T. and Madaeni, S.S. 2010. Experimental performance evaluation of polymeric membranes for treatment of an industrial oily wastewater. Desalination 262(1), 235-242.
Sarkar, B. 2015. Enhanced Cross-Flow Ultrafiltration of Apple Juice Using Electric Field. Journal of Food Processing and Preservation 39(6), 1372-1384.
Sarkar, B., DasGupta, S. and De, S. 2008. Effect of electric field during gel-layer controlled ultrafiltration of synthetic and fruit juice. Journal of Membrane Science 307(2), 268-276.
Sarkar, B. and De, S. 2011. Prediction of permeate flux for turbulent flow in cross flow electric field assisted ultrafiltration. Journal of Membrane Science 369(1), 77-87.
Shen, Y. and Badireddy, A.R. 2021. A Critical Review on Electric Field-Assisted Membrane Processes: Implications for Fouling Control, Water Recovery, and Future Prospects. Membranes 11(11), 820.
Song, W., Su, Y., Chen, X., Ding, L. and Wan, Y. 2010. Rapid concentration of protein solution by a crossflow electro-ultrafiltration process. Separation and Purification Technology 73(2), 310-318.
Sun, J., Hu, C., Tong, T., Zhao, K., Qu, J., Liu, H. and Elimelech, M. 2017. Performance and Mechanisms of Ultrafiltration Membrane Fouling Mitigation by Coupling Coagulation and Applied Electric Field in a Novel Electrocoagulation Membrane Reactor. Environmental Science & Technology 51(15), 8544-8551.
Ullah, A., Tanudjaja, H.J., Ouda, M., Hasan, S.W. and Chew, J.W. 2021. Membrane fouling mitigation techniques for oily wastewater: A short review. Journal of Water Process Engineering 43, 102293.
Venkataganesh, B., Maiti, A., Bhattacharjee, S. and De, S. 2012. Electric field assisted cross flow micellar enhanced ultrafiltration for removal of naphthenic acid. Separation and Purification Technology 98, 36-45.
Weng, Y.-H., Li, K.-C., Chaung-Hsieh, L.H. and Huang, C.P. 2006. Removal of humic substances (HS) from water by electro-microfiltration (EMF). Water Research 40(9), 1783-1794.
Yang, G.C.C., Yang, T.-Y. and Tsai, S.-H. 2003. Crossflow electro-microfiltration of oxide-CMP wastewater. Water Research 37(4), 785-792.
Zhang, Q., Arribas, P., Remillard, E.M., García-Payo, M.C., Khayet, M. and Vecitis, C.D. 2017. Interlaced CNT Electrodes for Bacterial Fouling Reduction of Microfiltration Membranes. Environmental Science & Technology 51(16), 9176-9183.
Zhao, C., Zhou, J., Yan, Y., Yang, L., Xing, G., Li, H., Wu, P., Wang, M. and Zheng, H. 2021. Application of coagulation/flocculation in oily wastewater treatment: A review. Science of The Total Environment 765, 142795.
Zhu, Z., Wei, Z., Sun, W., Hou, J., He, B. and Dong, Y. 2016. Cost-effective utilization of mineral-based raw materials for preparation of porous mullite ceramic membranes via in-situ reaction method. Applied Clay Science 120, 135-141.
Zou, D., Qiu, M., Chen, X., Drioli, E. and Fan, Y. 2019. One step co-sintering process for low-cost fly ash based ceramic microfiltration membrane in oil-in-water emulsion treatment. Separation and Purification Technology 210, 511-520.